HTML ABSTRACT + LINKS



# The Huggins band of ozone: A theoretical analysis

Zheng-Wang Qu, Hui Zhu, Sergy Yu. Grebenshchikov, and Reinhard Schinke[a)]
*Max-Planck-Institut für Strömungsforschung, D-37073 Göttingen, Germany*

Stavros C. Farantos
*Institute of Electronic Structure and Laser, Foundation for Research and Technology-Hellas, and Department of Chemistry, University of Crete, Iraklion 711 10, Crete, Greece*

(Received 13 August 2004; accepted 16 September 2004)

The Huggins band of ozone is investigated by means of dynamics calculations using a new (diabatic) potential energy surface for the $3\,^1A'(^1B_2)$ state. The good overall agreement of the calculated spectrum of vibrational energies and intensities with the experimental spectrum, especially at low to intermediate excitation energies, is considered as evidence that the Huggins band is due to the two $C_s$ potential wells of the $^1B_2$ state rather than the single $C_{2v}$ well of the $2\,^1A'(^1A_1)$ state. The vibrational assignment of the ''cold bands,'' based on the nodal structure of wave functions, on the whole supports the most recent experimental assignment [J. Chem. Phys. **115**, 9311 (2001)]. The quantum mechanical spectrum is analyzed in terms of classical periodic orbits and the structure of the classical phase space. © *2004 American Institute of Physics.* [DOI: 10.1063/1.1814098]

## I. INTRODUCTION

Because of the importance of ozone for the shielding of harmful UV light, its photophysics has been intensively studied.[1–3] Nevertheless, despite the enormous number of experimental and theoretical studies there are still several open questions, which wait for explanations. One of them concerns the electronic and vibrational assignment of the Huggins band ($310\ \text{nm} \lesssim \lambda \lesssim 370\ \text{nm}$). This absorption band, which was first observed more than a century ago,[4] is located at the red end of the strong Hartley band. The cross section is exceedingly small but increases by more than four orders of magnitude within the range of the Huggins band. It shows a long progression of diffuse vibrational structures, with the diffuseness gradually increasing with excitation energy. The assignment of the spectroscopic features in the Huggins band has been debated for a long time; a comprehensive résumé of the assignments suggested in the literature recently was given by O'Keeffe *et al.*[5] Several points make a clear-cut assignment of the Huggins band difficult: Doubts about the upper electronic state and therefore the topography of the relevant potential energy surface (PES), the diffuseness of the absorption features, and the congestion through hot bands, which are pronounced even at room temperature.

The upper electronic state in the transitions giving rise to the Huggins band can be either the second or the third singlet $^1A'$ state, $2\,^1A'(2\,^1A_1)$ or $3\,^1A'(1\,^1B_2)$, where the notations in parentheses give the electronic symmetry in $C_{2v}$ geometry; the ordering of states refers to the equilibrium geometry of the ground state $\tilde{X}\,^1A'(^1A_1)$ [see, for example, Fig. 1(b) in Ref. 6]. The second state, called $A$ according to Hay *et al.*,[7] has a single minimum—not taking into account the two additional equivalent minima arising due to exchange of the oxygen atoms; it is located at the $C_{2v}$ symmetry line ($R_1 = R_2$). The third state ($B$), on the other hand, has two $C_s$ minima with one bond length being substantially longer than the other one ($R_1 \approx 3.2\ a_0, R_2 \approx 2.3\ a_0$).[7–10] In what follows, $R_1$ and $R_2$ denote the bond distances between the central oxygen atom and the two outer ones and $\alpha$ is the OOO bond angle. States $A$ and $B$ have an avoided crossing in the energy range of the Huggins band. Both states asymptotically correlate with excited products, namely $O(^1D)$ and $O_2(a\,^1\Delta_g)$. They are crossed by a higher electronic state, usually referred to as $R$, which correlates with ground state products $O(^3P)$ and $O_2(X\,^3\Sigma_g^-)$. While the transition dipole moment function, $\mu$, with the ground state $X$ is very large for the $B$ state, it is very small for the $A$ state.[10,11] Both states are bound, in the sense that the energy at the equilibrium geometry is below the $O(^1D) + O_2(a\,^1\Delta_g)$ asymptote. However, their lifetimes are shortened by nonadiabatic transitions to the $R$ state or, to a lesser extend, to the several triplet states, which cross both states in the regions of their minima.[12]

Some authors[13–15] have suggested that the structures in the Huggins band are due to excitation of the vibrational states supported by the potential well of the $A$ state. In this case, the Huggins band would be weak because of the smallness of $\mu_{XA}$. However, the equilibrium of the $A$ state is not anywhere near the equilibrium of the ground state ($\alpha_e = 116.8°$), but has an equilibrium bond angle of 60°; the $A$ state correlates with cyclic ozone when the bond angle is varied.[10,16–18] Therefore, if the $A$ state were the origin of the Huggins band, a long progression in the bending mode should be expected, in contrast to what is observed experimentally.[5] Other authors[19–21] have suggested that the Huggins band is due to excitation of the vibrational states supported by the two $C_s$ wells of the $B$ state, i.e., that the weak Huggins band has the same electronic origin as the much stronger Hartley band. In this case, the Huggins band would be weak because of the large displacement between

a)Electronic mail: rschink@gwdg.de

 © 2004 American Institute of Physics

Downloaded 30 Nov 2004 to 139.91.254.18. Redistribution subject to AIP license or copyright, see http://jcp.aip.org/jcp/copyright.jsp

the equilibrium geometries of the $X$ and the $B$ state. The correct electronic assignment is important for a meaningful vibrational assignment of the diffuse structures. The topography of the two possible states is quite different and so is the expected vibrational dynamics: While for the $A$ state an assignment in terms of symmetric and antisymmetric stretch (normal) modes would be appropriate—as for the ground state of ozone—, such an assignment appears to be unreasonable in the $C_s$ wells of the $B$ state, in which the two O–O bonds are drastically different. In the latter case an assignment in terms of local modes is more meaningful.

A trustworthy interpretation of the diffuse structures in the Huggins band is only possible with dynamics calculations employing an accurate three-dimensional PES.[22] The electronic structure of the excited states of ozone is known to be complicated and with 24 electrons accurate *ab initio* calculations for constructing PESs are exceedingly time consuming. The first reliable investigation of the excited states of ozone is that of Hay and Dunning.[16] However, this work had been restricted to $C_{2v}$ geometries and therefore dissociation could not be studied. About five years later a full three-dimensional (3D) PES for the $B$ state was constructed by Sheppard and Walker.[23] This PES was based on electronic structure calculations in the interaction region by Hay *et al.*,[7] complemented by experimental information concerning the products. Although its general shape with two $C_s$ wells separated by a barrier appears qualitatively correct, it has not been used for explaining the Huggins band. About ten years later Yamashita *et al.*[8] (YMLL) and Le Quéré *et al.*[24] constructed a new global 3D $B$-state PES using calculated potential energies for approximately 80 geometries. The crossings of the $A$, $B$, and $R$ states have not been discussed in detail by these authors. The YMLL PES has two rather shallow $C_s$ wells with substantial barriers in the dissociation channels. About the same time, Banichevich *et al.*[9] calculated two-dimensional PESs for the $B$ state for three different bond angles; these surfaces are quite similar to the YMLL PES. The YMLL PES mainly has been exploited to study the photodissociation in the Hartley band of ozone.[24–26] It was also used, however, to calculate the eigenvalue spectrum of the shallow $C_s$ wells.[20,21] Although some qualitative aspects of the Huggins band were reproduced, these calculations left a number of questions unanswered, e.g., vibrational assignments, intensities, hot bands, and the actual types of vibrational motions associated with the stretching modes. We will compare these calculations to our results below. Incidentally we note, that O'Keeffe *et al.*[5] concluded that the Huggins band is due to absorption by the $A$ state. However, this assignment was made only because the energetics of the YMLL PES is in disagreement with experimental data.

Recently, we started to investigate the UV photodissociation of ozone again by calculating one- and two-dimensional cuts through the five lowest states of $^1A'$ symmetry.[10] Although the general behaviors of these cuts are similar to those obtained in the previous studies, marked quantitative differences have been found. Due to the increased computer power the new calculations could be performed on a higher level of electronic structure theory. In a second study[12] the investigation of Qu *et al.*[10] was complemented by calculating one-dimensional cuts also for the other symmetries, $^1A''$, $^3A'$, and $^3A''$, which allowed them to also discuss spin-forbidden processes. The calculations for the $^1A'$ states have been extended to include also the bending angle, i.e., full three-dimensional PESs have been calculated. In a first application we have constructed a 3D diabatic PES for the $B$ state and calculated the eigenvalue spectrum in the $C_s$ wells.[6] Although the agreement with the experimental spectrum is not perfect, it lead us to conclude with confidence that the Huggins band should be assigned to excitation of the $B$ state.

In this article we provide the details of the publication of Qu *et al.*[6] The *ab initio* and dynamics calculations are described in Secs. II and III, respectively. The results for $^{16}O_3$ and $^{18}O_3$ are presented and compared with the available experimental data for the Huggins band in Sec. IV. Additional information about the eigenvalue spectrum is obtained from an analysis of periodic classical orbits (Sec. V). The conclusions and suggestions for future work finish the article in Sec. VI.

## II. POTENTIAL ENERGY SURFACE AND TRANSITION DIPOLE MOMENT

### A. Electronic structure calculations

The electronic structure calculations for the 3D PESs of the $^1A'$ states are identical to those described by Qu *et al.*[10] The internally contracted multireference configuration interaction method with single and double excitations (MRD-CI) is used.[27,28] The preceding complete active space self-consistent field (CASSCF) calculations are performed with a full-valence active space with 18 electrons in 12 orbitals and with the three oxygen 1$s$ orbitals being doubly occupied but fully optimized. They are averaged over the five lowest $^1A'$ states leading to 4309 configurations with 8029 configuration state functions (CSFs). The fifth $^1A'$ state has been included in order to ensure that the lower four states ($X$, $A$, $B$, and $R$ in diabatic notation), which are the most important for describing the dissociation in the ultraviolet (UV) region, are well behaved. In the MRD-CI calculations all 18 valence electrons are correlated; however, the 6 electrons in the three oxygen 1$s$ orbitals are frozen. Dunning's augmented correlation consistent polarized valence triple zeta (aug-cc-pVTZ) basis set has been used throughout.[29] The most important configurations are selected with a 0.025 cut-off threshold for the norms of all CSFs and with at most 6 and 10 open shells in the reference and the internal space, respectively. This leads to about 90 reference configurations with 140 CSFs, or about 4 000 000 contracted configurations. The Davidson correction is applied in order to approximately account for higher-level excitations.[30] All calculations are carried out with the MOLPRO suite of programs.[31]

The two bond distances $R_1$ and $R_2$ and the bond angle $\alpha$ are used to define the 3D grid. One distance is varied between 1.9 $a_0$ and 3.4 $a_0$ with a step size of 0.1 $a_0$ and the other one between 1.9 $a_0$ and 8.0 $a_0$ with step sizes of 0.1 $a_0$, 0.25 $a_0$, 0.5 $a_0$, and 1.0 $a_0$ for the intervals [1.9,3.5], [3.5,4.5], [4.5,6.0], and [6.0,8.0], respectively. The angular grid ranges from 60° to 180° with $\Delta\alpha = 10°$. All

Downloaded 30 Nov 2004 to 139.91.254.18. Redistribution subject to AIP license or copyright, see http://jcp.aip.org/jcp/copyright.jsp

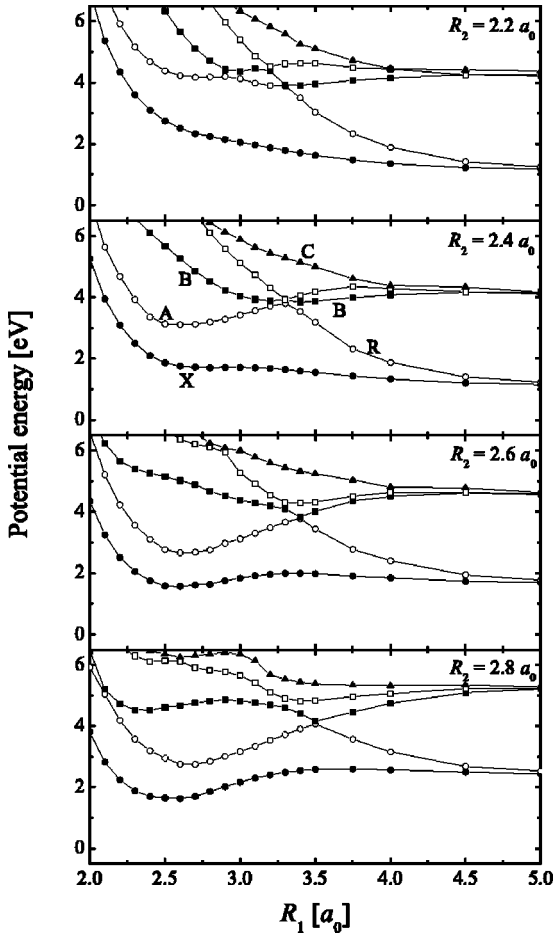


FIG. 1. One-dimensional cuts through the potential energy surfaces of the five lowest states of ozone with $^1A'$ symmetry. The adiabatic energies are depicted. Energy normalization is so that $E=0$ corresponds to the equilibrium of the ground state potential energy surface ($X$). $A$, $B$, $C$, and $R$ indicate the diabatic potential curves as discussed in the text. The bond angle is 90° and the O–O bond distance $R_2$ ranges from 2.2 $a_0$ to 2.8 $a_0$.

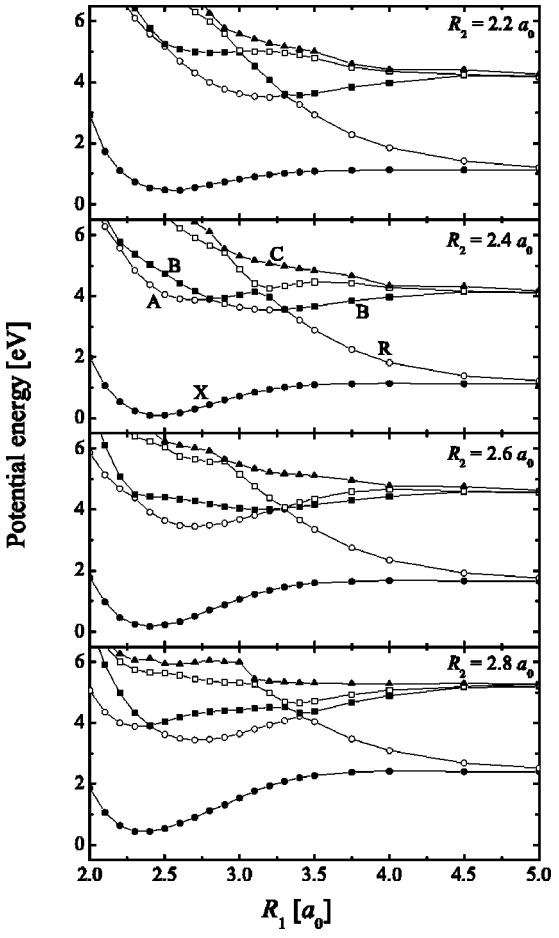


FIG. 2. The same as in Fig. 1, but for $\alpha=110°$.

potential energies quoted in this work are measured with respect to the equilibrium of the ground state PES.

One-dimensional cuts along the dissociation bond, $R_1$, for fixed O–O bond $R_2$ and bond angle $\alpha$ are depicted in Figs. 1–3. The data are the ''raw data'' as extracted from MOLPRO. Shown are the *adiabatic* energies, i.e., the symbols reflect the energetic ordering and not the character of the corresponding wave functions. Figures 1–3 clearly illustrate the complexity of the electronic structure of the $^1A'$ states. There are quite a number of avoided crossings; unlike conical intersections, these avoided crossings are not related to symmetry. At energies higher than ~6 eV there are additional avoided crossings, which, however, are not clearly seen when only five states are calculated (see, for example, the panels for $R_2=2.8\ a_0$). Even though the symbols indicate the adiabatic potential curves, it is not difficult to follow ''by eye'' *diabatic* potential curves, i.e., potential curves which are allowed to cross. The diabatic potentials are labeled by $X$ for the ground state, by $A$ and $B$ for the two states which are possibly excited in the Huggins–Hartley band system, by $R$ for the repulsive state, which crosses $A$ and $B$ leading to ground state products, and by $C$; the latter one is not involved in the UV photodissociation.

As already mentioned in Ref. 10 the patterns of avoided crossings depend sensitively on $R_2$ and $\alpha$. Important for the dynamics in the Huggins–Hartley band system are the crossings between $A$ and $B$, $A$ and $R$, and $B$ and $R$. For 110° and $R_2=2.2\ a_0$ these three crossings are well separated (Fig. 2). When $R_2$ is elongated they come closer and closer, both in terms of energy and in terms of the separation on the $R_1$ axis. For $R_2=2.6\ a_0$ the three states ''cross'' almost in one point. Although this general behavior is similar for the other two angles, displayed in Figs. 1 and 3, there are noticeable differences. Loosely speaking, the mixing between states $B$ and $R$, for example, indicated by the energy separation at the avoided crossing, is strongest for 90°. For $R_2=2.6\ a_0$ and 2.8 $a_0$ the spacing between the third and the forth curve ($B$ and $R$ in the diabatic sense) is so large that the adiabatic picture appears to be more reasonable than the diabatic one.

Ideally, one would like to do a three-state diabatization in order to determine three diabatic potentials $V_{ii}$ with $i=1-3$ and the corresponding coupling elements $V_{ij}$ with $i<j$. If the three avoided crossings are well separated such a procedure is feasible. However, when the curves cross in approximately a single point, the diabatization becomes much more involved.[32] Moreover, the MRD-CI calculations performed in this work are very time consuming and, therefore, diabatization calculations as implemented in the MOL-

Downloaded 30 Nov 2004 to 139.91.254.18. Redistribution subject to AIP license or copyright, see http://jcp.aip.org/jcp/copyright.jsp

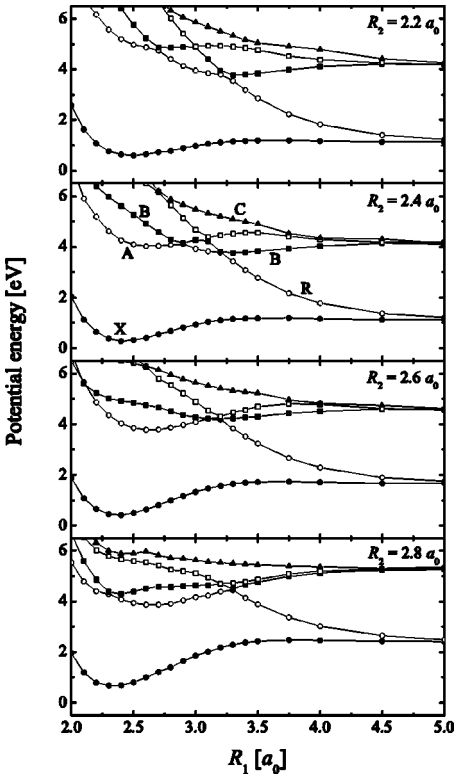


FIG. 3. The same as in Fig. 1, but for $\alpha = 130°$.

PRO suit of programs or which are based on the nonadiabatic coupling matrix elements[33,34] are beyond our practical possibilities at present time. For these reasons we decided to construct a diabatic *B*-state PES in the simplest way, i.e., by selecting appropriate points by eye in order to obtain smooth potential cuts. Examination of the main molecular orbital configurations as well as the transition dipole moments are also helpful for distinguishing points which belong to the diabatic *B* state. The purpose of the present work is an analysis of the Huggins band, i.e., the vibrational states in the shallow minima of the *B*-state PES which ranges from about 3.4 eV to about 4.2 eV. Within this energy range the mixing between *B* on one side and *A* and *R* on the other is rather small as compared to the higher energy regime and, therefore, this simplistic diabatization procedure appears to be reasonable. From excitation spectroscopy of jet-cooled ozone Sinha *et al.*[19] concluded that the homogeneous linewidth of single absorption lines is of the order of only 1 to 2 $cm^{-1}$. This indicates that the coupling between *B* and *A*/*R* is comparatively weak. However, the simple diabatization scheme is certainly not appropriate to study photodissociation in the Hartley band, where the nonadiabatic coupling is stronger.

Altogether about 1900 points in the angular interval $70° \leqslant \alpha \leqslant 140°$ have been selected for fitting the *B*-state PES; at smaller and larger angles the mixing is stronger and selecting appropriate points is not unambiguous. Incidentally we note, that a similar procedure has been applied by Hay *et al.*[7] for constructing the first *B*-state PES. Yamashita *et al.*[8] very likely followed the same procedure, although they did not explicitly mention how the avoided crossings have been treated in their construction of the *B*-state PES.

### B. Analytical fit of the *B*-state PES

The selected diabatic energies are fitted to an analytical expression of the Sorbie and Murrell type[35] according to

$$V(R_1,R_2,R_3) = a + D + V_I(R_1,R_2,R_3) + \sum_{i=1}^{3} v_i(R_i), \quad (1)$$

where the

$$v_i(R_i) = D[1 - e^{-\xi(R_i - R_e)}]^2 - D \quad (2)$$

are Morse potentials representing the asymptotic potential of $O_2(^1\Delta_g)$. The parameters $a = 4.045\,69$ eV, $D = 5.107\,84$ eV, $\xi = 1.341\,76\ a_0^{-1}$, and $R_e = 2.316\,45\ a_0$ are determined by least-squares fitting of the original data at an $O-O_2$ distance of $8\ a_0$. The parameter $a$ is the energy separation between the minimum of the *X*-state PES and the minimum of the $O(^1D) + O_2(a^1\Delta_g)$ asymptote. The three-body term is given by

$$V_I(R_1,R_2,R_3) = \prod_{i=1}^{3} [1 - \tanh(\beta R_i)] \sum_{l=1}^{31} C_l P_l^{kmn}(R_1,R_2,R_3). \quad (3)$$

The $P_l^{kmn}$ are combinations of polynomials $R_1^k R_2^m R_3^n$, which are fully symmetric in all three bond distances, with $0 \leqslant k + m + n \leqslant 7$. For example, for $k=3$, $m=3$, and $n=1$ the corresponding polynomial is

$$P^{331} = R_1^3 R_2^3 R_3^1 + R_1^1 R_2^3 R_3^3 + R_1^3 R_2^1 R_3^3,$$

and for $k=5$, $m=1$, and $n=0$ it is

$$P^{510} = R_1^5 R_2^1 + R_1^1 R_2^5 + R_2^5 R_3^1 + R_2^1 R_3^5 + R_3^5 R_1^1 + R_3^1 R_1^5.$$

The coefficients $C_l$ are determined by linear least-squares fitting and the parameter $\beta$ is adjusted "by hand" to ensure that the three-body term smoothly goes to zero when the dissociation channels are approached.

We performed two independent fits. In the first fit, termed $V_1$, all energies below 4 eV are given unit weight, while the points with higher energies are weighted with $\exp[-0.64(E_i - 4.0)^2] \leqslant 1$. In the second fit, termed $V_2$, all geometries are equally weighted. The parameters $\beta$ for $V_1$ and $V_2$ are 0.640 and 0.683, respectively, and the coefficients $C_l$ for both potentials are given in Table I. Distances are given in atomic units and potential energies in eV. The final PES is the combination of both fit potentials according to

$$V = \begin{cases} V_1 & \text{for } V_1 \leqslant 4.0 \text{ eV} \\ V_2 + \exp[-2(V_1 - 4)^2](V_1 - V_2) & \text{for } V_1 \geqslant 4.0 \text{ eV} \end{cases} \quad (4)$$

By combining the two fit potentials we accomplish that the fit is optimal in the region of the potential well and that the higher energies are still reasonably represented. The root mean square deviation of the fitted PES from the *ab initio* data is 0.033 eV for energies below 4 and 0.096 eV for all energies below 5 eV. When considering these deviations one has to keep in mind at least three aspects. First, the general quality of the electronic structure calculations, in which five states are determined simultaneously, is not as high as if, for example, only the ground state PES is calculated.[36] Second,

Downloaded 30 Nov 2004 to 139.91.254.18. Redistribution subject to AIP license or copyright, see http://jcp.aip.org/jcp/copyright.jsp

convergence problems in the *ab initio* calculations have been encountered at a substantial number of points. Curing these problems and, in addition, using the 0.025 cut-off threshold for selecting the configurations lead to some "noise" in the original data, which to some extent is smoothed by the analytic fit. Third, at higher energies the selection of potential energies for the diabatic potential is not unique.

The characteristic data of the fitted $B$-state PES are given in Table I of Ref. 6 and not repeated here. Two-dimensional contour plots are depicted in Fig. 4. There are six equivalent minima; however, in each of the two-dimensional cuts with one coordinate being fixed only two of them are observed. Qualitatively, the new PES looks similar to the older ones of Sheppard and Walker[23] and Yamashita *et al.*[8] Quantitatively, however, there are marked differences. For example, the YMLL PES has a substantial dissociation barrier, whereas our PES has only a tiny barrier of 8 meV.

### C. Transition dipole moment function

The MRD-CI calculations also yield the transition dipole moments of all excited states, $\vec{\mu}_{BX}$, $\vec{\mu}_{AX}$, etc., with the ground electronic state $X$. The out-of-plane component of $\vec{\mu}_{BX}$ is always zero. Because orientation and alignment effects are irrelevant for the present study, we take as transition dipole moment the absolute value of $\vec{\mu}_{BX}$. About 800 data points on the grid defined by $2.0\ a_0 \leqslant R_1 \leqslant 4.0\ a_0$, $2.0\ a_0 \leqslant R_2 \leqslant 2.7\ a_0$, and $90° \leqslant \alpha \leqslant 150°$ are used to fit the transition dipole moment function $\mu_{BX}$. At some geometries the mixing with the $A$ state leads to sharp structures of $\mu_{BX}$; they have been smoothed out, i.e., the diabatic transition dipole moment function is used rather than the adiabatic one. $\mu_{BX}$ is represented by

$$\mu_{BX}(R_1,R_2,R_3) = \exp\left(-2\sum_{i=1}^{3} S_i^2/\delta^2\right)\sum_{i=1}^{3} \exp(2S_i^2/\delta^2) \times \sum_{l=1}^{31} D_l P_l^{knm}(S_1,S_2,S_3), \quad (5)$$

where the polynomials are the same as used for representing the PES and $S_i = |R_i - R_0|$. The parameters $D_l$ are determined in a least-squares fitting procedure (Table I). The other parameters are $R_0 = 2.01\ a_0$ and $\delta = 1.21\ a_0^{-1}$. Both, the distances and the transition dipole moment function are given in atomic units. The analytical fit of the transition dipole moment function is valid only in the range of the original calculations. Two-dimensional contour plots of $\mu_{BX}$ are shown in Fig. 5. The $B$-state transition dipole moment is very large near the Franck–Condon (FC) point which explains why the Hartley band is so intense. Outside the FC region, towards large $O–O_2$ bond distances, $\mu_{BX}$ monotonically decreases.

TABLE I. Coefficients $C_l$ [Eq. (3)] and $D_l$ [Eq. (5)] for the two fitted potential energy surfaces of the $B$ state of ozone, $V_1$ and $V_2$, and the $B \leftarrow X$ transition dipole moment function, $\mu_{BX}$.

| $l$ | $k$ | $m$ | $n$ | $V_1$ | $V_2$ | $\mu_{BX}$ |
|---|---|---|---|---|---|---|
| 1 | 0 | 0 | 0 | 2.619 364 768 (8)[a] | 4.627 009 628 (8) | 0.507 685 58 |
| 2 | 1 | 0 | 0 | −1.721 347 776 (8) | −3.961 061 679 (8) | −2.091 338 29 |
| 3 | 2 | 0 | 0 | 5.088 978 416 (7) | 1.191 169 029 (8) | 3.950 932 00 |
| 4 | 1 | 1 | 0 | 9.682 077 595 (7) | 3.165 947 114 (8) | 4.594 128 19 |
| 5 | 3 | 0 | 0 | −9.137 272 745 (6) | −1.442 033 133 (7) | −1.547 017 65 |
| 6 | 2 | 1 | 0 | −2.106 654 115 (7) | −8.664 188 953 (7) | −6.289 755 73 |
| 7 | 1 | 1 | 1 | −6.310 582 37 (7) | −2.353 821 967 (8) | −4.642 083 16 |
| 8 | 4 | 0 | 0 | 1.831 610 654 (6) | 7.449 363 789 (5) | −0.944 883 11 |
| 9 | 3 | 1 | 0 | 5.335 228 361 (5) | 8.631 404 515 (6) | 5.845 912 64 |
| 10 | 2 | 2 | 0 | 5.305 783 116 (6) | 2.161 574 084 (7) | 1.182 689 88 |
| 11 | 2 | 1 | 1 | 1.386 233 081 (7) | 5.791 867 504 (7) | 4.312 697 79 |
| 12 | 5 | 0 | 0 | −3.299 724 41 (5) | −1.884 772 856 (3) | 1.104 751 71 |
| 13 | 4 | 1 | 0 | 2.255 516 569 (5) | −3.494 130 129 (5) | −2.946 678 42 |
| 14 | 3 | 2 | 0 | −3.425 715 755 (5) | −1.825 312 53 (6) | −0.488 731 19 |
| 15 | 3 | 1 | 1 | −4.375 927 815 (5) | −4.177 812 58 (6) | −4.887 498 55 |
| 16 | 2 | 2 | 1 | −3.237 289 176 (6) | −1.292 027 098 (7) | 3.884 306 77 |
| 17 | 6 | 0 | 0 | 2.899 723 573 (4) | −1.459 059 723 (4) | −0.417 228 99 |
| 18 | 5 | 1 | 0 | −6.881 109 763 (3) | 4.550 226 504 (4) | 0.933 947 89 |
| 19 | 4 | 2 | 0 | −3.872 194 051 (4) | −1.684 293 455 (4) | −0.080 057 47 |
| 20 | 4 | 1 | 1 | −6.704 142 029 (4) | 2.541 757 206 (4) | 1.581 160 76 |
| 21 | 3 | 3 | 0 | 8.163 498 885 (4) | 2.231 880 805 (5) | 0.349 188 53 |
| 22 | 3 | 2 | 1 | 1.350 192 862 (5) | 7.229 860 368 (5) | −1.802 232 89 |
| 23 | 2 | 2 | 2 | 7.616 442 142 (5) | 2.651 266 023 (6) | 1.278 983 75 |
| 24 | 7 | 0 | 0 | −1.309 103 501 (3) | −5.452 074 795 (1) | 0.057 280 88 |
| 25 | 6 | 1 | 0 | 1.318 900 233 (3) | 3.248 667 18 (3) | −0.140 570 48 |
| 26 | 5 | 2 | 0 | −2.039 899 391 (2) | −6.350 394 249 (3) | 0.060 931 50 |
| 27 | 5 | 1 | 1 | −6.418 476 888 (3) | −2.610 919 034 (4) | −0.049 597 95 |
| 28 | 4 | 3 | 0 | −5.539 203 62 (2) | 4.376 899 134 (1) | −0.040 298 29 |
| 29 | 4 | 2 | 1 | 1.658 704 857 (4) | 3.705 444 988 (4) | 0.039 493 30 |
| 30 | 3 | 3 | 1 | −2.130 091 596 (4) | −7.269 750 732 (4) | 0.513 986 65 |
| 31 | 3 | 2 | 2 | −2.932 003 575 (4) | −1.064 214 972 (5) | −0.002 950 00 |

[a]Numbers in parentheses indicate powers of ten.

Downloaded 30 Nov 2004 to 139.91.254.18. Redistribution subject to AIP license or copyright, see http://jcp.aip.org/jcp/copyright.jsp

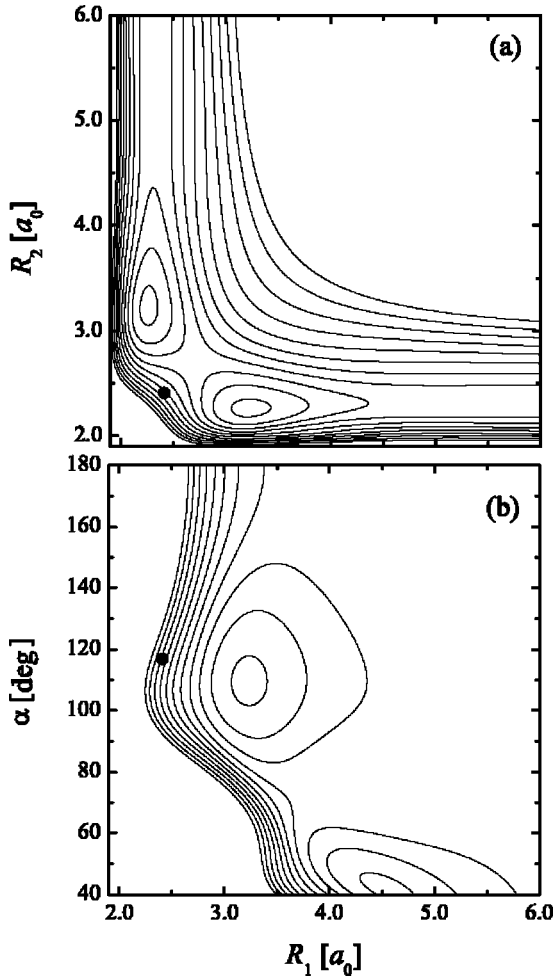


FIG. 4. (a) Contour plot of the *B*-state potential energy surface as function of the two bond distances for fixed bond angle $\alpha=110°$. The highest contour is 6 eV and the energy spacing is 0.25 eV. The dot marks the Franck–Condon point. (b) Contour plot as function of one bond distance and the bond angle; the other bond distance is fixed at 2.3 $a_0$. Other details are the same as in (a).

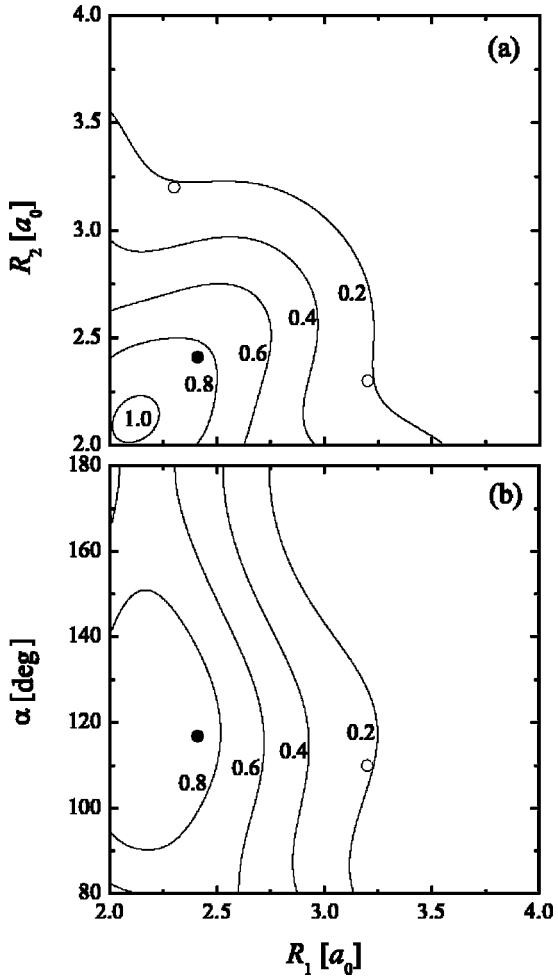


FIG. 5. (a) Contour plot of the transition dipole moment function $\mu_{BX}$ as function of the two bond distances for fixed bond angle $\alpha=110°$. The contours are in atomic units. The full circle marks the Franck–Condon point and the open circles indicate the minima of the *B*-state PES. (b) Contour plot of the transition dipole moment function $\mu_{BX}$ as function of one bond distance and the bond angle; the other bond distance is fixed at 2.3 $a_0$. The other details are the same as in (a).

The FORTRAN codes for calculating the PES and the transition dipole moment function can be obtained from one of the authors (Schinke).

## III. DYNAMICS CALCULATIONS

Because of the permutation symmetry there are three equivalent ozone conformers for $^{16}O_3$ and $^{18}O_3$. Two of them can be seen in Fig. 4(b), one near $\alpha=110°$ and the other one near $\alpha=40°$. Since there exists a sizable barrier along the shortest connection between the wells belong to different conformers, it suffices to perform the calculations for a single conformer. The path with the lowest energy from one conformer to another one runs via the $O+O_2$ asymptote, i.e., the minimal energy between two conformers is the dissociation energy. In the present study, however, energies only up to the dissociation energy are considered. In order to take the $C_{2v}$ symmetry of each conformer into account the dynamics calculations are performed using ''symmetric'' Jacobi coordinates: $R$ is the distance from the central oxygen atom to the center-of-mass of the two end atoms, $r$ is the distance between the two end atoms, and $\gamma$ denotes the angle between the vectors **R** and **r**. These coordinates were previously employed for the calculation of vibrational–rotational states in the ground electronic state[36,37] or for the photodissociation of ozone in $^3B_2$ electronic state.[38] The Hamiltonian in these coordinates is symmetric with respect to the exchange of the two end atoms, i.e., it is symmetric with respect to $\gamma=90°$. Thus, the eigenstates are either symmetric or antisymmetric with respect to $\gamma=90°$. The energy difference between the symmetric and the corresponding antisymmetric states represents the tunneling splitting between the two $C_s$ wells of the *B*-state PES. This symmetry can be incorporated in the numerical grid in the same way as was done, e.g., for ozone in the *X* state.[37]

All calculations are for zero total angular momentum. The discrete variable representation[39] (DVR) is used to represent the Hamiltonian matrix. Typically, the following grid parameters are adopted: $0.5\ a_0 \leqslant R \leqslant 3.0\ a_0$ with 64 potential optimized points[40] and $3.0\ a_0 \leqslant r \leqslant 7.0\ a_0$ with 64 potential optimized points. The angular coordinate is represented by 64 Gauss–Legendre quadrature points[41] in the interval 0

Downloaded 30 Nov 2004 to 139.91.254.18. Redistribution subject to AIP license or copyright, see http://jcp.aip.org/jcp/copyright.jsp

$\leqslant\gamma\leqslant 90°$. Only those points are retained in the grid, whose potential energy is smaller than 6.5 eV.

Two types of dynamics calculations have been performed: Filter diagonalization[42,43] and harmonic inversion.[44] In the filter diagonalization method first an appropriate set of basis functions is generated in a small energy window by applying a filtering operator onto an initial wave packet. In the second step, the Hamiltonian is then diagonalized in the sub-space of this energy-adapted basis functions. The eigenfunctions are explicitly provided by the calculation and can be analyzed in terms of their nodal structures. Calculations are performed in a set of narrow energy windows in order to cover a larger range of energies. Intensities $I_n^{(i)}$ are determined as

$$I_n^{(i)}=|\langle\Phi_i^X|\mu_{BX}|\Psi_n^B\rangle|^2, \tag{6}$$

where $\Phi_i^X$ and $\Psi_n^B$ are vibrational wave functions in the $X$ and the $B$ state, respectively.

In the harmonic inversion approach an initial wave packet $\mu_{BX}\Phi_i^X$ is propagated and the eigenenergies and intensities are obtained by signal processing of the Chebychev autocorrelation function $\{c_n\}$, i.e., the overlap of the initial wave packet with the Chebychev vector at iteration $n$. No basis functions have to be stored and therefore the harmonic inversion method requires much less core memory than the filter diagonalization method. For this reason, considerably larger grids with more grid points can be used. Because the density of states is small, no convergence problems have been encountered in the analysis. In order to obtain intensities for different initial vibrational states $i$ in the $X$ state different initial wave packets have to be propagated. It has been checked that both methods yield the same results. The deviations in the energies are smaller than 0.1 $cm^{-1}$ and the intensities typically agree within a few percent.

Incidentally we note, that the tunneling splitting between symmetric and antisymmetric states is negligibly small. For the relatively high energy window from 3.90 to 3.92 eV the maximum splitting is of the order of only 0.02 $cm^{-1}$. In the present study we consider only absorption from the (0,0,0) ground state in the $X$ state, which is symmetric. Therefore, only the symmetric states in the $B$ state are of relevance; the corresponding antisymmetric states have zero overlap. If the initial state in the ground electronic state is antisymmetric, i.e., $v_3$ is odd, the reverse is true.

## IV. RESULTS

### A. Energies, wave functions, and assignments

We have calculated the vibrational eigenstates of $^{16}O_3$ and $^{18}O_3$ up to about 4.1 eV; for comparison, the equilibrium energy is 3.429 eV and the energy of the quantal (classical) dissociation limit is 4.136 eV (4.046 eV).[6] All wave functions have been visually inspected using a three-dimensional plotting routine in order to assign quantum numbers $(v_1,v_2,v_3)$. The quantum numbers refer to only one of the $C_s$ wells. $v_1$ counts the nodes along the long O–O bond, $v_2$ is the bending quantum number, and $v_3$ refers to excitation of the short O–O bond. In all previous studies $v_1$ and $v_3$ were assigned to symmetric and antisymmetric stretch motion, respectively. Such an interpretation of the modes is not reasonable for a molecule in which the two bond lengths differ by a factor of roughly 1.4. The excitation energies (with respect to the ground vibrational state in the $B$ state) are listed in Tables II and III together with the assignments. The bending frequency is the smallest while the short-bond stretch frequency is the largest. The ratio of the three fundamental frequencies is approximately 2:1:4, i.e., one quantum of the $\nu_1$ ($\nu_3$) mode is worth two (four) quanta of the bending mode. However, with increasing excitation this ratio tends to 2:1:5 (see below). Also shown in Tables II and III are the relative intensities (normalized with respect to the ground vibrational state).

The progression of pure bending states, $(0,v_2,0)$, is very long. We followed it only up to $v_2=12$, but very likely it continues almost unperturbed to even higher excitations. The corresponding wave functions for several members of this progression are depicted in Fig. 6 as functions of $R$ and $r$. The corresponding two-dimensional cut of the PES is shown in the first panel of the same figure. The third coordinate, $\gamma$, is chosen so that the potential energy is minimal for a particular set $(R,r)$; in this way the dissociation channel when both $R$ and $r$ become large is visible. Of the three possible two-dimensional planes, $(R,r)$, $(R,\gamma)$, and $(r,\gamma)$, the first one is best suited to illustrate excitation of the bending as well as the long-bond stretching mode. The pure bending states do not lead to dissociation. They avoid the FC region and their separation from it remains more or less the same which explains why their intensities do not change much from $v_2=0$ to 12 (Tables II and III).

The pure long-bond stretch progression, $(v_1,0,0)$, also can be followed without problems to high excitations. Examples of the corresponding wave functions are depicted in Fig. 7. Up to $v_1=4$ the wave functions are very clear and not significantly perturbed. With (5,0,0), however, systematic mixing with another type of states sets in. The wave functions for (6,0,0) and (7,0,0) seem to consist of two different branches, one which is almost independent of $r$ and another one in which both $r$ and $R$ elongate simultaneously. On the first glance, the wave functions of the $(v_1,0,0)$ states advance towards the dissociation channel as $v_1$ increases. This is expected for the mode in which the long O–O bond, that is, the dissociation bond is excited. However, a more careful examination shows that the backbones of the wave functions for $v_1\leqslant 4$ do not exactly point to the transition state (TS) barrier in the dissociation channel (see the first panel in Fig. 7), but are slightly deflected from it. This is probably a consequence of the 2:1 resonance between the long-bond stretching and the bending mode.[45] The $(R,r)$ dependent branches of the (6,0,0) and (7,0,0) wave functions do point towards the TS in the dissociation channel. This change of the qualitative structure of the higher members of the long-bond stretching progression illustrates the gradual increase of mixing with states that do lead to dissociation. More detailed discussions are given in Sec. V of this article and especially in Ref. 46.

With increasing excitation the wave functions of the $(v_1,0,0)$ states extend further and further in the direction of the FC point with the result that the overlap with the $(0,0,0)_X$

Downloaded 30 Nov 2004 to 139.91.254.18. Redistribution subject to AIP license or copyright, see http://jcp.aip.org/jcp/copyright.jsp

TABLE II. Assignments, transition energies, deviations from experimental transition energies, and relative intensities [for excitation from the vibrational ground state $(0,0,0)_X$] of the calculated vibrational states for $^{16}O_3$.

| no. | $(v_1,v_2,v_3)$ | $\Delta E$ | exp.−cal. | $I$ | no. | $(v_1,v_2,v_3)$ | $\Delta E$ | exp.−cal. | $I$ |
|---|---|---|---|---|---|---|---|---|---|
| 1 | 000 | 0[a] | | 1.0 | 46 | 340 | 3291.5 | −74 | 343.6 |
| 2 | 010 | 386.6 | | 1.0 | 47 | 051 | 3344.6 | | 59.1 |
| 3 | 100 | 702.4 | 3 | 9.3 | 48 | 260 | 3363.1 | | 196.6 |
| 4 | 020 | 766.8 | | 1.0 | 49 | 180 | 3440.7 | | 88.8 |
| 5 | 110 | 1071.6 | −15 | 11.6 | 50 | 301 | 3441.5 | | 1417.8 |
| 6 | 030 | 1140.5 | | 0.9 | 51 | 510 | 3467.3 | −70 | 95.3 |
| 7 | 200 | 1373.9 | −21 | 42.6 | 52 | 430 | 3510.0 | −52 | 1683.3 |
| 8 | 120 | 1434.2 | | 13.8 | 53 | 0100 | 3522.1 | | 1.8 |
| 9 | 001 | 1495.0 | | 3.0 | 54 | 221 | 3528.6 | | 64.1 |
| 10 | 040 | 1507.0 | | 0.7 | 55 | 102 | 3569.5 | | 2.2 |
| 11 | 210 | 1724.7 | −34 | 64.5 | 56 | 350 | 3582.8 | | 932.8 |
| 12 | 130 | 1789.7 | | 15.4 | 57 | 141 | 3604.3 | | 9.6 |
| 13 | 050 | 1865.7 | | 1.3 | 58 | 022 | 3656.4 | | 53.1 |
| 14 | 011 | 1879.2 | | 2.9 | 59 | 270 | 3661.0 | | 247.8 |
| 15 | 300 | 2012.5 | −42 | 120.9 | 60 | 061 | 3693.4 | | 1.8 |
| 16 | 220 | 2068.4 | −34 | 90.3 | 61 | 600 | 3695.5 | −83 | 6.2 |
| 17 | 140 | 2137.7 | | 18.4 | 62 | 520 | 3732.0 | −54 | 1337.0 |
| 18 | 101 | 2181.6 | | 39.1 | 63 | 190 | 3740.0 | | 41.7 |
| 19 | 060 | 2216.5 | | 1.1 | 64 | 311 | 3779.0 | | 3582.0 |
| 20 | 021 | 2256.7 | | 3.1 | 65 | 440 | 3803.7 | −66 | 119.9 |
| 21 | 310 | 2343.4 | −43 | 211.6 | 66 | 0110 | 3819.0 | | 3.1 |
| 22 | 230 | 2404.7 | | 115.2 | 67 | 231 | 3849.5 | | 1594.6 |
| 23 | 150 | 2477.6 | | 21.2 | 68 | 360 | 3874.9 | | 249.1 |
| 24 | 111 | 2547.7 | | 56.8 | 69 | 112 | 3926.4 | | 199.3 |
| 25 | 070 | 2558.4 | | 0.8 | 70 | 151 | 3933.2 | | 228.7 |
| 26 | 400 | 2615.5 | −67 | 226.6 | 71 | 610 | 3939.9 | −53 | 233.6 |
| 27 | 031 | 2627.1 | | 1.3 | 72 | 280 | 3953.8 | | 111.1 |
| 28 | 320 | 2666.9 | −55 | 339.4 | 73 | 530 | 3992.8 | −46 | 2781.1 |
| 29 | 240 | 2733.0 | | 147.9 | 74 | 1100 | 4017.4 | | 115.9 |
| 30 | 160 | 2808.6 | | 26.3 | 75 | 032 | 4023.0 | | 0.3 |
| 31 | 201 | 2831.4 | | 285.1 | 76 | 401 | 4038.4 | | 3347.1 |
| 32 | 080 | 2890.6 | | 1.8 | 77 | 071 | 4038.9 | | 148.3 |
| 33 | 002 | 2897.5 | | 2.0 | 78 | 450 | 4061.9 | −70 | 2303.8 |
| 34 | 121 | 2910.4 | | 30.2 | 79 | 0120 | 4101.4 | | 7.6 |
| 35 | 410 | 2925.5 | −63 | 446.9 | 80 | 321 | 4106.4 | | 2413.9 |
| 36 | 330 | 2981.7 | −58 | 382.5 | 81 | 370 | 4136.8 | | 1352.9 |
| 37 | 041 | 2991.0 | | 77.6 | 82 | 700 | 4152.5 | −71 | 472.6 |
| 38 | 250 | 3052.4 | | 183.6 | 83 | 202 | 4158.2 | | 33.7 |
| 39 | 170 | 3130.0 | | 31.7 | 84 | 241 | 4180.4 | | 406.1 |
| 40 | 500 | 3173.2 | −76 | 53.6 | 85 | 620 | 4193.7 | −58 | 6.3 |
| 41 | 211 | 3185.9 | | 908.0 | 86 | 290 | 4216.3 | | 499.4 |
| 42 | 090 | 3212.2 | | 1.6 | 87 | 003 | 4238.9 | | 1101.9 |
| 43 | 420 | 3225.3 | −60 | 380.3 | 88 | 540 | 4244.6 | −48 | 1845.7 |
| 44 | 131 | 3256.2 | | 320.5 | 89 | 161 | 4263.2 | | 1.4 |
| 45 | 012 | 3282.5 | | 182.3 | | | | | |

[a]Absolute energy: 3.595 eV.

ground-state wave function and, therefore, the absorption intensity rapidly increases, at least up to $v_1=4$. This behavior is interrupted at state (5,0,0). The intensity drops to a minimum at $v_1=6$ and then it rises again. It appears plausible to assume that this qualitative change of the behavior of the intensity with $v_1$ is caused by the changes of the $(v_1,0,0)$ wave functions discussed above, although the pictures in Fig. 7 do not provide clear clues. Because the intensities are exceedingly small, they are sensitive probes of the structure of the wave functions; a very small change may have a drastic implication.

Because of the large frequency, which is close to the frequency of the free $O_2$ molecule, the $(0,0,v_3)$ progression is short; only the states $v_3=1-3$ are in the energy range considered. Excitation of the short-bond stretch is best seen in projections on the planes $(R,\gamma)$ or $(r,\gamma)$. While state (0,0,1) is rather pure, the overtones $v_3=2$ and 3 are gradually more perturbed. Since excitation of the short O–O bond does not shorten the distance to the FC point, excitation of the $v_3$ bond by one and two quanta does not increase the intensity substantially. However, because of mixing with some ''bright'' state the intensity of (0,0,3) is large. The nature of this perturbing state is not clear. All states in the immediate vicinity of (0,0,3), like (6,2,0), (2,9,0), and (5,4,0), are well behaved. A possible candidate for mixing with (0,0,3) is state (2,0,2). It is $\sim 80\ \mathrm{cm}^{-1}$ lower in energy, but the change in quantum numbers is small.

The $(v_1,v_2,0)$ combination states are all very clear and

Downloaded 30 Nov 2004 to 139.91.254.18. Redistribution subject to AIP license or copyright, see http://jcp.aip.org/jcp/copyright.jsp

TABLE III. Assignments, transition energies, deviations from experimental transition energies, and relative intensities [for excitation from the vibrational ground state $(0,0,0)_X$] of the calculated vibrational states for $^{18}O_3$.

| no. | $(v_1,v_2,v_3)$ | $\Delta E$ | exp.−cal. | $I$ | no. | $(v_1,v_2,v_3)$ | $\Delta E$ | exp.−cal. | $I$ |
|---|---|---|---|---|---|---|---|---|---|
| 1 | 000 | 0[a] | | 1.0 | 46 | 340 | 3135.2 | −64 | 787.0 |
| 2 | 010 | 365.3 | | 1.1 | 47 | 051 | 3168.8 | | 45.6 |
| 3 | 100 | 664.6 | 20 | 10.0 | 48 | 260 | 3203.4 | | 303.5 |
| 4 | 020 | 725.0 | | 1.1 | 49 | 301 | 3273.2 | | 2048.5 |
| 5 | 110 | 1014.6 | −8 | 13.3 | 50 | 180 | 3277.1 | | 43.1 |
| 6 | 030 | 1078.8 | | 1.1 | 51 | 510 | 3307.1 | −64 | 24.2 |
| 7 | 200 | 1301.9 | −12 | 50.3 | 52 | 221 | 3339.7 | | 2345.5 |
| 8 | 120 | 1358.6 | | 16.4 | 53 | 0100 | 3354.4 | | 1.9 |
| 9 | 001 | 1414.8 | | 3.6 | 54 | 430 | 3360.6 | −53 | 414.2 |
| 10 | 040 | 1426.6 | | 0.9 | 55 | 102 | 3386.3 | | 18.9 |
| 11 | 210 | 1635.7 | −24 | 79.2 | 56 | 141 | 3411.6 | | 1072.2 |
| 12 | 130 | 1696.5 | | 19.0 | 57 | 350 | 3425.8 | | 389.6 |
| 13 | 050 | 1767.4 | | 1.7 | 58 | 022 | 3466.2 | | 0.2 |
| 14 | 011 | 1778.0 | | 3.5 | 59 | 270 | 3490.0 | | 404.2 |
| 15 | 300 | 1910.3 | −33 | 157.1 | 60 | 061 | 3502.1 | | 23.1 |
| 16 | 220 | 1963.2 | −34 | 114.3 | 61 | 600 | 3534.5 | −79 | 0.1 |
| 17 | 140 | 2027.9 | | 23.1 | 62 | 190 | 3566.9 | | 132.5 |
| 18 | 101 | 2065.6 | | 47.9 | 63 | 520 | 3568.1 | −49 | 3237.5 |
| 19 | 060 | 2101.4 | | 1.4 | 64 | 311 | 3597.6 | | 2687.8 |
| 20 | 021 | 2135.1 | | 4.1 | 65 | 440 | 3630.8 | −64 | 2145.4 |
| 21 | 310 | 2226.7 | −41 | 283.9 | 66 | 0110 | 3643.0 | | 3.2 |
| 22 | 230 | 2284.2 | | 149.3 | 67 | 231 | 3661.0 | | 1079.9 |
| 23 | 150 | 2352.2 | | 27.0 | 68 | 360 | 3698.9 | | 1268.7 |
| 24 | 111 | 2412.9 | | 71.7 | 69 | 112 | 3726.8 | | 179.4 |
| 25 | 070 | 2427.8 | | 1.3 | 70 | 151 | 3738.1 | | 98.2 |
| 26 | 031 | 2486.3 | | 15.8 | 71 | 280 | 3772.0 | | 464.5 |
| 27 | 400 | 2487.7 | −57 | 315.1 | 72 | 610 | 3777.6 | −57 | 772.0 |
| 28 | 320 | 2536.5 | −44 | 465.0 | 73 | 032 | 3811.5 | | 0.1 |
| 29 | 240 | 2598.3 | | 194.8 | 74 | 530 | 3823.9 | −45 | 5042.5 |
| 30 | 160 | 2669.0 | | 34.0 | 75 | 071 | 3824.1 | | 1876.6 |
| 31 | 201 | 2684.9 | | 358.0 | 76 | 1100 | 3847.0 | | 26.1 |
| 32 | 080 | 2745.8 | | 4.3 | 77 | 401 | 3847.6 | | 991.3 |
| 33 | 002 | 2747.2 | | 11.3 | 78 | 450 | 3885.8 | −56 | 7411.3 |
| 34 | 121 | 2757.8 | | 56.3 | 79 | 321 | 3911.2 | | 505.0 |
| 35 | 410 | 2785.4 | −49 | 642.9 | 80 | 0120 | 3919.6 | | 5.7 |
| 36 | 041 | 2830.6 | | 7.1 | 81 | 370 | 3955.3 | | 3399.2 |
| 37 | 330 | 2839.9 | −54 | 649.6 | 82 | 202 | 3956.6 | | 351.5 |
| 38 | 250 | 2904.9 | | 246.5 | 83 | 241 | 3980.3 | | 8.5 |
| 39 | 170 | 2977.6 | | 40.7 | 84 | 700 | 3992.8 | −73 | 174.8 |
| 40 | 211 | 3015.4 | | 467.7 | 85 | 003 | 4023.5 | | 722.9 |
| 41 | 500 | 3032.6 | −72 | 770.6 | 86 | 620 | 4026.5 | −51 | 57.3 |
| 42 | 090 | 3055.1 | | 2.2 | 87 | 290 | 4031.9 | | 1138.0 |
| 43 | 420 | 3074.0 | −49 | 575.5 | 88 | 161 | 4053.1 | | 162.7 |
| 44 | 131 | 3088.1 | | 563.8 | 89 | 122 | 4069.3 | | 168.5 |
| 45 | 012 | 3112.4 | | 44.8 | 90 | 540 | 4077.1 | −44 | 6713.0 |

[a]Absolute energy: 3.586 eV.

unambiguously assignable. The same is valid for the $(0,v_2,v_3)$ and, mostly, for the $(v_1,0,v_3)$ states. Generally speaking, perturbations are largest if all three modes are simultaneously excited. What has been said about the $^{16}O_3$ spectrum is generally true also for $^{18}O_3$ and, therefore, a detailed discussion of its eigenvalue spectrum is skipped. There is, however, one quantitative difference: In contrast to $^{16}O_3$ the change in the intensities for progression $(v_1,0,0)$ occurs at $v_1=6$ rather than 5. This shows that the effect leading to the qualitative change in the spectrum sensitively depends on dynamical details, e.g., the atomic masses.

### B. Comparison with experiment

The comparison between experimental and calculated vibrational transition energies is based on the energies and assignments given in Table I of O'Keeffe *et al.*[5] The experimental energies are those of Katayama[47] whereas the assignments are those of O'Keeffe *et al.*[5] Only the "cold bands" are taken into account in the comparison; our assignment of the "hot bands" differs from that of O'Keeffe *et al.*[5] as will be discussed elsewhere.[48] For $^{16}O_3$ the ground vibrational state of the excited state has a transition energy (measured with respect to the lowest vibrational state in the ground electronic state) of 27 112 $cm^{-1}$. The corresponding energy for $^{18}O_3$ has not been given. Using the calculated zero-point energies for $^{16}O_3$ and $^{18}O_3$ in the $X$ state[36] and the same data for the $B$ state calculated in the present work, a value of 27 115 $cm^{-1}$ is estimated. (The entries for $^{18}O_3$ in Table I of Ref. 5 are misaligned; this failure has been cor-

Downloaded 30 Nov 2004 to 139.91.254.18. Redistribution subject to AIP license or copyright, see http://jcp.aip.org/jcp/copyright.jsp

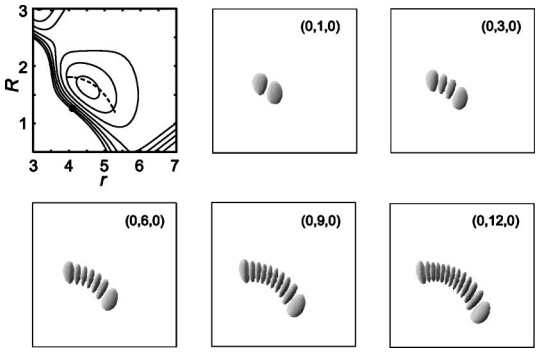


FIG. 6. Wave functions of the pure bending states $(0,v_2,0)$ for $v_2=1$, 3, 6, 9, and 12. Shown is one particular contour $\epsilon(R,r,\gamma)=|\Psi(R,r,\gamma|^2$ with the value of $\epsilon$ being the same for all panels. The plots are viewed along the $\gamma$ axis, in the direction perpendicular to the $(R,r)$ plane. Shading emphasizes the 3D character of the wave functions. The first panel shows the PES as function of $R$ and $r$ (in $a_0$); for each $(R,r)$ the third coordinate, $\gamma$, is chosen so that the potential energy is minimal. The full circle marks the FC point and the dashed line indicates a classical periodic orbit of the bending family, $B1A$ in Fig. 9.

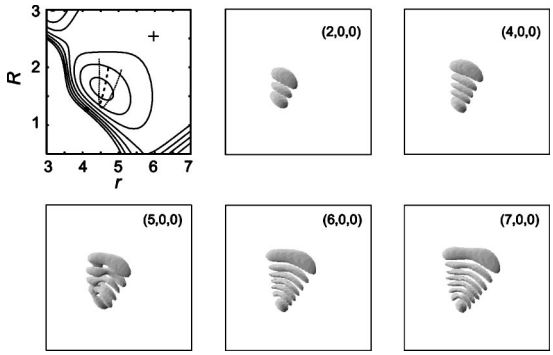


FIG. 7. Wave functions of the pure long-bond stretching states $(v_1,0,0)$ for $v_2=2$, and 4–7. All other details are the same as in Fig. 6. The cross in the first panel marks the small barrier in the dissociation channel. The dashed line indicates a classical periodic orbit of the $S1$ family in Fig. 9 and the dotted line represents a periodic orbit of the $S1A$ family.

rected in accordance with one of the authors of Ref. 5, T.R.) Tables II and III give the differences of the experimental and calculated vibrational transition energies.

The agreement of the calculated excitation energies with the experimental ones is good. The average deviation is $53\ \mathrm{cm}^{-1}$ for $^{16}O_3$ and $48\ \mathrm{cm}^{-1}$ for $^{18}O_3$. In view of the limited level of electronic structure theory, the very crude ''diabatization'' procedure, and the neglect of nonadiabatic transitions to the $A$ and $R$ states (or the many triplet states), the success of the present calculations is notable. The deviations gradually increase with energy. The agreement appears even better if we consider separations between neighboring states of individual progressions. Examples are given for the pure $v_1$ progression and the $(v_1,v_2,0)$ progressions for several $v_1$ in Table IV.

However, the kind of comparison between experimental and theoretical excitation energies as presented in Tables II–IV is questionable: It is not clear whether the theoretical state (5,0,0), for example, corresponds to the state which is termed (5,0,0) in the assignment by O'Keeffe *et al.*[5] The theoretical assignment is based on the wave functions and it is for the majority of states listed in Tables II–IV unique. The experimental assignment, on the other hand, is based on energy separations and intensities, i.e., the development of progressions from low to high energies. There is no guarantee that the two assignments agree. A more faithful comparison of experiment and theory requires to consider also the real absorption spectrum, i.e., the intensity pattern.

Figure 8 shows the measured absorption spectrum at a temperature of 218 K.[49] The vertical lines above the spectrum indicate the transition energies measured by Katayama[47] together with the assignments of O'Keeffe *et al.*;[5] the solid and dashed lines indicate ''cold'' and ''hot'' bands, respectively. The hot bands will not be discussed in this work. Because the long-bond stretching frequency is roughly twice the bending frequency, the measured spectrum is approximately organized in groups or polyads with ''polyad quantum number'' $P=2v_1+v_2$; states with the same $P$ have roughly the same energy. From $P=0$ to $P=15$ the spectrum increases by almost four orders of magnitude. Beyond the energy range shown in the main body of Fig. 8, i.e., $P\geqslant 15$, the spectrum rapidly becomes very diffuse as illustrated in the inset of Fig. 8. Above $P=18$, corresponding to $v_1=9$, hardly any resolved structures are observable. This is in accord with the experimental dissociation limit for the $B$ state being $32\,316\ \mathrm{cm}^{-1}$.[50] While below this limit shortening of the lifetime is only possible due to predissociation, mainly through coupling with the $R$ state, above the dissociation threshold direct bond breaking on the $B$-state PES is expected to be the dominant process. Because the $v_1$ mode is supposedly the dissociation bond, direct excitation of this mode leads to very short lifetimes corresponding to broad resonance structures in the absorption cross

TABLE IV. Separations (in $\mathrm{cm}^{-1}$) between neighboring states of different progressions for $^{16}O_3$.

| | | $v_2$, $E_{(v_1,v_2,0)}-E_{(v_1,v_2-1,0)}$ | | | | |
|---|---|---|---|---|---|---|
| $v_1$ | $E_{(v_1,0,0)}-E_{(v_1-1,0,0)}$ | 1 | 2 | 3 | 4 | 5 |
| 1 | 702 (706[a,b]) | 369 (351) | | | | |
| 2 | 672 (647) | 351 (338) | 344 (343) | | | |
| 3 | 639 (617) | 331 (330) | 323 (312) | 315 (312) | 310 (293) | |
| 4 | 603 (578[b]) | 310 (314) | 300 (303) | 285 (293) | 294 (280) | 258 (254) |
| 5 | 558 (549) | 294 (300) | 265 (281) | 261 (269) | 252 (250) | |
| 6 | 522 (515) | 244 (275) | 254 (249) | | | |

[a]Numbers in parenthesis are the experimental values as quoted in Ref. 5.
[b]This number is different from the corresponding number in Table II of Ref. 5.

Downloaded 30 Nov 2004 to 139.91.254.18. Redistribution subject to AIP license or copyright, see http://jcp.aip.org/jcp/copyright.jsp

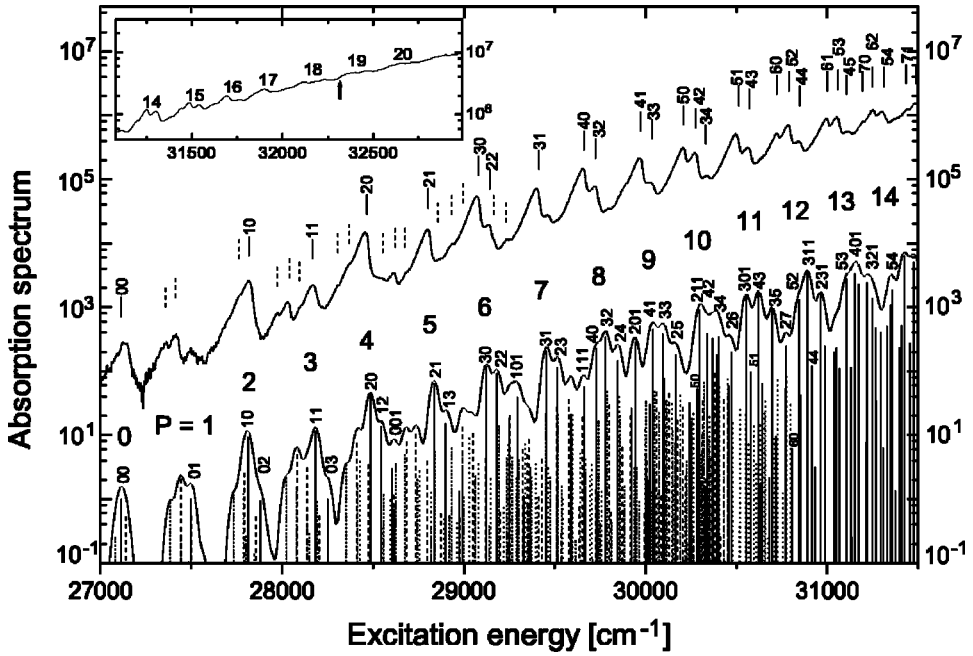


FIG. 8. The absorption cross section of $^{16}O_3$ in the region of the Huggins band (arbitrary units). The continuous curve in the upper part represents the measured cross section of Malicet *et al.* for 218 K (Ref. 49). The numbers above the experimental spectrum give the assignments of the cold bands due to O'Keeffe *et al.* (Ref. 5); the dashed vertical lines indicate hot bands (not discussed in this work). $P=1,2,\ldots$ is the polyad quantum number $2v_1+v_2$. The inset shows the continuation of the measured spectrum to higher excitation energies; the arrow marks the experimental dissociation limit. The stick spectrum in the lower part depicts the calculated intensities $I_n^{(i)}$ for excitation from the the ground vibrational state in the $X$ state ($i=0$); they are normalized so that $I_{(0,0,0)}^{(0)}=1$. If only two quantum numbers are given, $v_3$ is equal to zero. The broken vertical lines in the lower part of the figure represent the hot bands originating from vibrational states (0,1,0) (dotted lines), (0,0,1) (long-dash lines), and (1,0,0) (short-dash lines), respectively, in the ground electronic state. The intensities include the appropriate Boltzmann factors for a temperature of 250 K. Not all hot bands are shown for energies above 30 500 $cm^{-1}$. The continuous line is the broadened spectrum according to Eq. (7). The theoretical spectrum is shifted so that the (0,0,0) band agrees with the experimental origin at 27 112 $cm^{-1}$.

section.[22,51] Up to $P=10$ the $(P/2,0,0)$ state has the largest intensity within its polyad. Beyond $P=10$ the intensity pattern changes and state $((P-2)/2,2,0)$ is more intense (see also Table II of Ref. 5). The spectrum is quite regular and the assignment given by O'Keeffe *et al.*[5] without excitation of the third mode seems to be plausible.

There are a few lines in the measured spectrum, which apparently are not included in the results of Katayama[47] and, therefore, are not assigned by O'Keeffe *et al.*[5] One is the peak around 27 500 $cm^{-1}$, which according to our calculations should be the fundamental of the bending progression. The peak near 29 500 $cm^{-1}$ is probably state (2,3,0). Two very weak bands not assigned by O'Keeffe *et al.* are seen just above band (3,2,0). Whether they belong to the cold or the hot bands is not clear.

The lower part of Fig. 8 depicts the calculated stick spectrum. There are four different sets of lines according to four vibrational states in the electronic ground state from which absorption originates: $i=0$ for $(0,0,0)_X$, $i=1$ for $(1,0,0)_X$, $i=2$ for $(0,1,0)_X$, and $i=3$ for $(0,0,1)_X$. The corresponding vibrational excitation energies $\omega_X^{(i)}$ (in $cm^{-1}$) are 0, 1103.1, 700.9, and 1042.1 for $i=1-4$.[52] The calculated relative intensities $I_n^{(i)}$ for $i=0$ are given in Table II; the intensities for absorption originating from the excited states in the ground electronic state ($i=1-3$) will be given in Ref. 48. The ''sticks'' shown in the lower part of Fig. 8 include the Boltzmann factors $g_T^{(i)}=e^{-\omega_X^{(i)}/kT}$, where $k$ is Boltzmann's constant; the temperature is chosen to be 250 K. The calculated energy[6] for the $(0,0,0)_B \leftarrow (0,0,0)_X$ transition is 27 520 $cm^{-1}$ compared to the measured energy[5] of 27 112 $cm^{-1}$. In order to facilitate the comparison, the calculated spectrum is shifted on the energy axis so that the (0,0,0) bands coincide.

In the following we consider only the cold lines, i.e., those originating from $(0,0,0)_X$ ($i=0$). In the low energy range the relationship between the measured and the calculated lines is unique and even the intensity ratios are reasonably well reproduced. For example, states (0,0,0) and (0,1,0) have about the same intensity both in the measured and the calculated spectrum. The intensities for states (1,0,0) and (1,1,0) are also similar and roughly an order of magnitude larger than for states (0,0,0) and (0,1,0). For polyads $P=4-7$ the calculated intensity patterns still reproduce the experimental patterns. Starting with state (4,0,0), however, the intra-polyad intensity ratios are in qualitative disagreement with the corresponding experimental rations. For example, in polyad $P=8$ of the experimental spectrum the intensity for (4,0,0) is larger than the (3,2,0) intensity; the opposite is true, however, for the calculated spectrum.

The relationship between experiment and calculation becomes truly questionable with state (5,0,0), i.e., polyad $P=10$. The intensity for (5,0,0) is very small in the calculation. On the other hand the intensity for state (2,1,1), which is almost degenerate with (5,0,0), is large. Above $P=10$ more and more states with $v_3=1$ are seen in the calculated spectrum, whereas the experimental one can be assigned

Downloaded 30 Nov 2004 to 139.91.254.18. Redistribution subject to AIP license or copyright, see http://jcp.aip.org/jcp/copyright.jsp

TABLE V. Comparison of vibrational excitation energies for $^{16}O_3$ from two different calculations.

| $(v_1,v_2,v_3)$ | This work | Ref. 21 | $(v_1,v_2,v_3)$ | This work | Ref. 21 |
|---|---|---|---|---|---|
| 000 | 0 | 0[a] | 210 | 1725 | 1598 |
| 010 | 387 | 402 | 130 | 1790 | 1740 |
| 100 | 702 | 640 | 050 | 1866 | 1889 |
| 020 | 767 | 793 | 011 | 1879 | 1807[b] |
| 110 | 1072 | 1023 | 300 | 2012 | 1771 |
| 030 | 1140 | 1171 | 220 | 2068 | 1936 |
| 200 | 1374 | 1234 | 140 | 2138 | 2074 |
| 120 | 1434 | 1389 | 101 | 2182 | 2008[b] |
| 001 | 1495 | 1425[b] | 060 | 2216 | 2227 |
| 040 | 1507 | 1537 | 021 | 2257 | 2173[b] |

[a]Only the states with $A_1$ symmetry are considered.
[b]The quantum number $v_3$ of Ref. 21 has been divided by 2.

without excitation in the third mode. The states with $v_3=1$ can be integrated into the polyad structure if we assume, at intermediate and high energies, an approximate 2:1:5 resonance, i.e., if the polyad quantum number is defined as $P=2v_1+v_2+5v_3$.

In the theoretical stick spectrum above polyad $P=10$ more and more states with $v_3=1$ have large intensities while the importance of states with $v_3=0$ becomes smaller. This is the result of the qualitative change of the theoretical spectrum around $P=10$, which apparently has a large impact on the wave function overlaps. As a consequence, the number of states with similar intensities in a polyad increases. For example, polyad $P=13$ contains five bands with similar intensities. On the other hand, photofragment excitation (PHOFEX) spectra recorded in jet-cooled beams[53,54] show only two bands for $P=13$, (6,1,0) and (5,3,0). Because rotational broadening is largely eliminated, the PHOFEX spectra are very clean with band widths of the order of 20 $cm^{-1}$. The severe disagreement with the theoretical spectrum for $P=13$ (as well as for larger polyads) clearly indicates the limitation of the dynamics calculations, particularly of the PES. For polyads larger than $P=12$ or so the calculated spectrum is not trustworthy. The simplicity of the PHOFEX spectra, which have been measured only for $P=12-15$[53] and for $P=9-15$,[54] respectively, calles for a simple assignment with only $v_3=0$ states.[5] If also states with $v_3=1$ were excited, the spectrum very likely would be more complicated.

In order to make the comparison between the experimental and the calculated spectrum slightly more realistic we generate a continuous spectrum by broadening each line with a Gaussian according to

$$\sigma(E)=\sum_{i=0}^{3} g_T^{(i)} \sum_n I_n^{(i)} \exp\{-\kappa[E-(E_n-\omega_X^{(i)})]^2\}. \quad (7)$$

The exponent $\kappa$ determines the full width at half maximum (FWHM) of the Gaussian. It is supposed to represent both coherent broadening due to predissociation and incoherent broadening due to the averaging over many rotational transitions. From the jet-cooled excitation spectra[19] and PHOFEX spectra[53,54] it is clear that the latter is the dominant effect.[55] The result for a FWHM of 50 $cm^{-1}$ and $T=250$ K is shown in the lower part of Fig. 8.

The overall agreement of the synthesized spectrum with the measured one is reasonable. The general increase of the average spectrum with energy is quite similar in both cases. Moreover, the organization in terms of well separated polyads is clearly visible, even at higher energies. The gap between the polyads is generally deeper in the calculated spectrum, but that is not unexpected in view of the simplistic modeling of coherent and incoherent broadening. The qualitative appearance of polyad $P=10$ in the theoretical spectrum is not dissimilar with that in the measured spectrum and the same is true also for the higher polyads—despite the fact that the underlying transitions in the measured and the calculated spectra are different.

### C. Comparison with previous calculations

There are two dynamical studies of the spectrum in the Huggins band prior to ours, both employing the YMLL PES.[20,21] While Le Quéré and Leforestier[20] performed a time-dependent wave packet analysis, Bludský and Jensen[21] calculated the eigenvalue spectrum by a time-independent approach similar to our study. The latter authors also analyzed the nodal pattern of the wave functions and provided an assignment in terms of symmetric stretch, bending, and asymmetric stretch quantum numbers. For the states symmetric with respect to the $C_{2v}$ plane their $v_3'$ is two times our $v_3$; likewise, for the states antisymmetric with respect to the $C_{2v}$ plane their $v_3'$ is $2v_3+1$. As mentioned above, we do not think that an interpretation in terms of symmetric stretch and asymmetric stretch motion is appropriate for the $C_s$ wells of ozone in the Huggins band.

The results of Bludský and Jensen[21] are compared to the present results in Table V. The dissociation energy of the YMLL PES is much lower than for our PES and, therefore, only the lowest five states are bound states; the others are resonances. However, because of the substantial dissociation barrier the lifetimes of these resonances are very long and, therefore, the lower resonance states also can be considered as bound states. The ordering of the lowest twelve states is identical to the ordering of our results. With state (0,5,0), however, the two orderings of states become different. The two bending frequencies (387 and 402 $cm^{-1}$) are similar with the result that even the higher bending overtones have similar excitation energies. The short-bond stretch frequencies (1495 and 1425 $cm^{-1}$) differ by about 70 $cm^{-1}$ or less than 5%. Most drastic are the (relative) differences for the long-bond stretch frequency (702 and 640 $cm^{-1}$). As a consequence of the much lower dissociation energy $\omega_1$ for the YMLL PES is substantially smaller than for our PES. Therefore, the higher overtones $(v_1,0,0)$ have much too small excitation energies. Thus, while the general structure of the spectrum is qualitatively correct, at least for low excitation energies, a quantitative comparison with the experimental energies is impossible.

Le Quéré and Leforestier[20] calculated the absorption spectrum (by Fourier transformation of the autocorrelation function) and compared it with an experimental (stick) spectrum. An assignment of the underlying wave functions has not been done and therefore the assignment of Brand *et al.*[56]

Downloaded 30 Nov 2004 to 139.91.254.18. Redistribution subject to AIP license or copyright, see http://jcp.aip.org/jcp/copyright.jsp

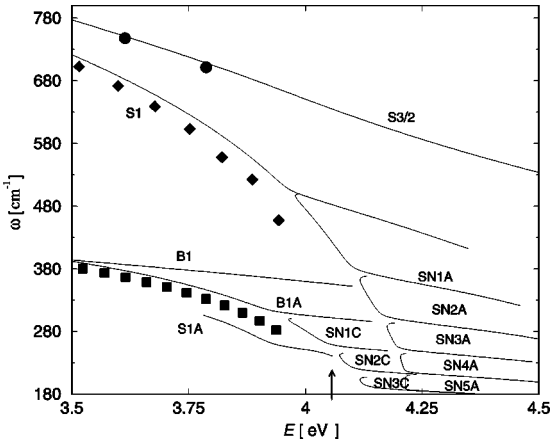


FIG. 9. Continuation/bifurcation diagram as obtained from the analysis of the classical phase space. The solid lines represent the frequencies of the periodic orbits for five different families as described in the text: $B1$, $B1A$ (bending); $S1$, $S1A$ (long-bond stretch); $S3$ (short-bond stretch). The SNiA and SNiC indicate saddle-node bifurcations. The symbols represent the energy spacings between neighboring states of the overtone progressions $(0,v_2,0)$ (■), $(v_1,0,0)$ (◆), and $(0,0,v_3)$ (●), respectively. The frequencies for the short-bond stretch are divided by two. The $S1A$ family originates from a period-doubling bifurcation of the $S1$ family, i.e., its frequency is half the $S1$ frequency at the bifurcation point. The arrow on the energy axis marks the energy of the transition state barrier in the dissociation channel. For more details see the text.

of the data of Simons *et al.*[57] has been adopted. This assignment involves excitations of one and two quanta of the third mode. The calculated spectrum qualitatively agrees with the measured intensities in that it rapidly increases with energy. Because no assignment of the calculated lines has been done, comparison with the results of Bludský and Jensen[21] as well as our results is not unambiguous.

## V. PERIODIC ORBITS AND CONTINUATION/ BIFURCATION DIAGRAM

In many applications it has been demonstrated that the development of the quantum mechanical spectrum of eigenstates can be explained and elucidated by an analysis of the classical phase space.[45,58] For this purpose, one finds families of periodic orbits (POs) and follows them as a function of energy, which yields the so-called continuation/bifurcation (CB) diagram.[59] The motions described by the POs can be compared with the quantum mechanical wave functions of the vibrational overtone states.

The $B$-state PES of ozone has six equivalent minima of $C_s$ symmetry and several saddle points which separate these minima. From each minimum a number of families of stable POs emanate, at least as many as the number of normal modes. At higher energies we find POs by applying continuation techniques.[60] The stability analysis of each PO reveals the behavior of trajectories in the vicinity of this particular PO. This approach traces those critical energies at which one observes qualitatively different types of motions associated with bifurcations, i.e., the appearance of new types of POs. One way to represent a CB diagram is to plot the periods ($\tau$) or the frequencies ($\omega=2\pi/\tau$) of the POs as functions of the total energy.[58,61,62] The resulting CB diagram for the Huggins band of ozone is shown in Fig. 9.

The continuous lines in Fig. 9 denote the frequencies of POs as functions of the total energy $E$. The families denoted by $B1$, $S1$, and $S3$ correspond to the bending, the long-bond stretch, and the short-bond stretch modes, respectively. For simplicity of the representation the frequency of the $S3$ family is divided by two. The harmonic frequencies at the bottom of the potential well are $\omega_1=743\ \mathrm{cm}^{-1}$, $\omega_2=400\ \mathrm{cm}^{-1}$, and $\omega_3=1585\ \mathrm{cm}^{-1}$. They are in an approximate 2:1:4 resonance. The $S1A$ family is a bifurcation of the $S1$ family at 3.781 eV; the corresponding POs have periods which are twice the periods of the POs of the parent family $S1$ (period-doubling bifurcation).

In previous studies[58,61,62] we have found that saddle-node (SN) bifurcations are a frequent type of bifurcation in molecular systems. They are important because at SN bifurcations new types of molecular motions abruptly come into existence which do not exist at lower energies. The newly created stable POs may be embedded in chaotic regions of the phase space. Often they allow the molecule to access regions of the configuration space, for example, dissociation or isomerization channels, which the POs starting from the bottom of the potential do not access.

The $B1$ family of POs exhibits a very early SN bifurcation, $B1A$, at 3.475 eV, just slightly above the bottom of the potential well. The two most anharmonic families, $S1$ and $B1A$, both develop cascades of SN bifurcations as the energy approaches the dissociation barrier; they are termed SNiA and SNiC, respectively. The cascadelike structure of SN bifurcations seen in Fig. 9 is typical for molecular systems at high energies.[58,61–64] When the slope of $\omega$ of a particular mode suddenly changes new families of POs are generated and one branch resumes the highly anharmonic branch, which already existed below the bifurcation. As energy increases the frequency again levels off and a new SN bifurcation takes place. This behavior is the consequence of gradually switching on and off of high-order resonances as the energy varies. Although it is difficult to follow the high-order resonances, it turns out that the cascades of SN bifurcations converge to some critical energies, which are clearly higher than the tiny barrier to dissociation marked by the arrow in Fig. 9. This underlines that the pure long-bond stretch mode does not directly lead to dissociation as was already noted above in connection with the $(v_1,0,0)$ wave functions. Another series of SN bifurcation exists, which is associated with the $S1A$ family. This SN bifurcation gives birth to POs which do lead to dissociation. A more detailed account of this phenomenon will be given elsewhere.[46]

Examples of POs for the $B1A$, $S1$, and $S1A$ families are shown in the first panels of Figs. 6 and 7, respectively. The $B1A$ PO clearly coincides with the backbones of the bending wave functions. Likewise, the $S1$ orbit closely follows the $(v_1,0,0)$ wave functions, at least for $v_1\leqslant 4$. However, the stretching wave functions for $v_1\geqslant 5$ seem to be influenced by both the $S1$ and the $S1A$ POs.

The classical frequencies are compared with the energy differences between adjacent quantum levels for the three overtone progressions (1,0,0), (0,1,0), and (0,0,1), respectively. The energy differences are plotted with respect to the upper level. In order to approximately account for the zero-

Downloaded 30 Nov 2004 to 139.91.254.18. Redistribution subject to AIP license or copyright, see http://jcp.aip.org/jcp/copyright.jsp

point energy, the quantum results are shifted to lower energies by the zero-point energy. This shift is not rigorously founded and affects the quantitative comparison with the classical frequencies. Nevertheless, the agreement is reasonable for the entire energy range considered. Especially the anharmonicities, which are not affected by the shift by the zero-point energy, are well reproduced by the classical calculations. Interestingly, the bending overtones follow the anharmonic branch of the SN family, $B1A$, rather than the $B1$ family.

In closing this section we underline that most of the families of POs which have been located remain stable up to the dissociation limit. At higher energies they become single unstable, that is, unstable in one degree of freedom. From this point of view, one cannot consider the dynamics of ozone in its $B$ state, even at energies close to the dissociation threshold, to be highly chaotic. The existence of stable POs up to high energies is in accord with the clear-cut assignability of the majority of wave functions up to the dissociation limit.

## VI. DISCUSSION, CONCLUSIONS, AND OUTLOOK

We have performed electronic structure calculations for the first five $^1A'$ states of ozone on a level of theory which exceeds all previous calculations for this system; all three internal coordinates have been involved. From these calculations a three-dimensional diabatic potential energy surface (PES) for the $B$ state, i.e., the second excited state at the ground-state equilibrium, has been constructed. Although this PES is qualitatively similar to previously published PESs, there are distinctive differences: The potential well is significantly deeper and a dissociation barrier is practically missing. This PES has been used to calculate the eigenenergies and wave functions in the two $C_s$ wells. Franck–Condon factors with the vibrational states in the electronic ground state, including the transition dipole moment function, have also been determined. Almost all vibrational states up to the (calculated) dissociation threshold ($4363\ \mathrm{cm}^{-1}$) can be uniquely assigned in terms of three modes: The long-bond stretching mode ($v_1$), the bend ($v_2$), and the short-bond stretching mode ($v_3$).

Despite the fact that both the electronic structure and the dynamics calculations are of limited accuracy—relatively small atomic basis, selection of most important configurations, neglect of nonadiabatic coupling among the different electronic states, extremely simplistic diabatization—the agreement with the experimental absorption spectrum is on the whole good. Up to polyad quantum number $P=2v_1+v_2=9$ corresponding to about 70% of the dissociation energy, the relationship between the calculated and the measured spectrum is unique and the agreement is quantitative. Starting with $P=10$ ($v_1=5$) the relationship between experiment and calculations is not unique any longer. This observation coincides with the change of the nature of the ($v_1$,0,0) wave functions and the change of the corresponding intensities. The monotonic increase of the intensities is interrupted between $v_1=4$ and 5 and, as a consequence, the most intense peak in the $P=10$ polyad is attributed to state (2,1,1) whereas in the experimental spectrum it is assigned as (5,0,0). This kind of ambiguity exists for all higher polyads. In view of the simplicity of the jet-cooled PHOFEX spectra we are confident, however, that the assignment of O'Keeffe *et al.*[5] is preferrable.

Qualitative and systematic changes of wave functions as the dissociation threshold is approached is common in molecular systems.[45] They are related to bifurcations, primarily saddle-node bifurcations, in the classical phase space, that is, they are the result of non-linear couplings in the Hamiltonian. Indeed, the classical phase space analysis shows that the dynamics becomes drastically more complex close to the threshold.[46] For our potential the wave function changes occur at about 60%–70% of $D_0^{(\mathrm{PES})}=4363\ \mathrm{cm}^{-1}$. The experimental dissociation energy is $D_0^{(\mathrm{exp})}=5204\ \mathrm{cm}^{-1}$ and thus about $850\ \mathrm{cm}^{-1}$ larger. From the experimental spectrum it is difficult to suspect whether a systematic change of the wave functions does happen in reality. We note, however, that the intensity pattern of the ($v_1$,0,0) peaks changes between $v_1=6$ and 7 (Table II in Ref. 5; see also Fig. 8). From $v_1=1$ through 6 it rises while from 7 onward the intensity decreases again, i.e., the intensities for the long-bond progression show a behavior which is—at least qualitatively—similar to that observed in the calculations. $v_1=6$ and 7 correspond to roughly 70% and 80% of $D_0^{(\mathrm{exp})}$. Whether this change has the same origin as the similar change observed in the calculations is not definite. However, qualitative changes of the eigenfunctions close to the dissociation threshold are very likely to occur. Incidentally we note, that also the PHOFEX spectrum of O'Keeffe *et al.*[54] becomes more complicated above polyad $P=15$.

In the present work we discussed exclusively the cold bands in the 218 K absorption spectrum. In a forthcoming publication[48] we will discuss the hot bands; they are pronounced in the Huggins band. With increasing temperature new structures appear, in comparison with the 218 K spectrum, in the low-energy range of the Huggins band. It will be shown that these structures are due to excitations from ground state vibrational levels with two quanta of stretching excitation, i.e., (0,0,2) and (1,0,1). All structures in the lower part of the 295 K spectrum can be uniquely assigned. Because of unfavorable FC factors, excitations from state (2,0,0) are only marginally reflected in the spectrum.

In view of the good agreement of our calculations with the experimental spectra, for both the cold and the hot vibrational bands, we conclude that a long standing puzzle is resolved: The Huggins band of ozone is due to excitation of the $B$ state, i.e., the same state as excited in the Hartley band; the absorption features are due to excitation of the vibrational states in the two wells with $C_s$ symmetry. Secondly, the vibrational modes seen in the spectrum are, primarily, the long-bond stretch and the bend. Theory suggests that at higher excitations also the short-bond stretch is excited. However, this conclusion might be a shortcoming of the PES used in the dynamics calculations, whose dissociation energy is by about 0.1 eV too small compared to the measured dissociation energy. Future electronic structure calculations on a higher level of theory (larger atomic basis sets, a smaller cutoff threshold for the configuration state functions, etc.) may correct this underestimation. Preliminary calculations in

Downloaded 30 Nov 2004 to 139.91.254.18. Redistribution subject to AIP license or copyright, see http://jcp.aip.org/jcp/copyright.jsp

which only three states are averaged over in the CASSCF approach indicate a substantial increase of the dissociation energy.

One important drawback of the present calculations is the neglect of nonadiabatic coupling of the $B$ state to the other two important states with $^1A'$ symmetry, namely $A$ and $R$. Calculations which incorporate all three electronic states are in preparation. They will yield not only the positions of the vibrational bands but also the lifetimes and, therefore, the widths of the individual vibrational bands, which can be compared with the experimental estimates of Sinha *et al.*[19] Nevertheless, the smallness of the linewidths in the jet-cooled excitation spectra as well as the good agreement with the experimental absorption spectrum, at least for lower energies, indicates that the diabatic model is reasonable.

## ACKNOWLEDGMENTS

Financial support by the Deutsche Forschungsgemeinschaft is gratefully acknowledged. The authors are grateful to Dr. Malicet for providing the experimental absorption cross section shown in Fig. 8. R.S. acknowledges valuable discussions with T. Ridley on the Huggins band.

[1] P. L. Houston, in *Advanced Series in Physical Chemistry. Modern Trends in Chemical Reaction Dynamics; Experiment and Theory*, edited by X. Yang and K. Liu. (World Scientific, Singapore, 2004).
[2] J. Orphal, J. Photochem. Photobiol., A **157**, 185 (2003).
[3] Y. Matsumi and M. Kawasaki, Chem. Rev. (Washington, D.C.) **103**, 4767 (2003).
[4] W. Huggins and Mrs. Huggins , Proc. R. Soc. London **48**, 216 (1890).
[5] P. O'Keeffe, T. Ridley, K. P. Lawley, and R. J. Donovan, J. Chem. Phys. **115**, 9311 (2001).
[6] Z.-W. Qu, H. Zhu, M. Tashiro, R. Schinke, and S. C. Farantos, J. Chem. Phys. **120**, 6811 (2004).
[7] P. J. Hay, R. T. Pack, R. B. Walker, and E. J. Heller, J. Phys. Chem. **86**, 862 (1982).
[8] K. Yamashita, K. Morokuma, F. Le Quéré, and C. Leforestier, Chem. Phys. Lett. **191**, 515 (1992).
[9] A. Banichevich, S. D. Peyerimhoff, and F. Grein, Chem. Phys. **178**, 155 (1993).
[10] Z.-W. Qu, H. Zhu, and R. Schinke, Chem. Phys. Lett. **377**, 359 (2003).
[11] M. H. Palmer and A. D. Nelson, Mol. Phys. **100**, 3601 (2002).
[12] H. Zhu, Z.-W. Qu, M. Tashiro, and R. Schinke, Chem. Phys. Lett. **384**, 45 (2004).
[13] J. A. Joens, J. Chem. Phys. **101**, 5431 (1994).
[14] K. Takahashi, M. Kishigami, N. Taniguchi, Y. Matsumi, and M. Kawasaki, J. Chem. Phys. **106**, 6390 (1997).
[15] A. Banichevich and S. D. Peyerimhoff, Chem. Phys. **174**, 93 (1993).
[16] P. J. Hay and T. H. Dunning, Jr., J. Chem. Phys. **67**, 2290 (1977).
[17] G. J. Atchity and K. Ruedenberg, Theor. Chem. Acc. **96**, 176 (1997).
[18] R. Siebert and R. Schinke, J. Chem. Phys. **119**, 3092 (2003).
[19] A. Sinha, D. Imre, J. H. Goble, Jr., and J. L. Kinsey, J. Chem. Phys. **84**, 6108 (1986).
[20] F. Le Quéré and C. Leforestier, Chem. Phys. Lett. **189**, 537 (1992).
[21] O. Bludský and P. Jensen, Mol. Phys. **91**, 653 (1997).
[22] R. Schinke, *Photodissociation Dynamics* (Cambridge University Press, Cambridge, 1993).
[23] M. G. Sheppard and R. B. Walker, J. Chem. Phys. **78**, 7191 (1983).
[24] C. Leforestier, F. Le Quéré, K. Yamashita, and K. Morokuma, J. Chem. Phys. **101**, 3806 (1994).
[25] N. Balakrishnan and G. D. Billing, J. Chem. Phys. **101**, 2968 (1997).
[26] M. Alacid and C. Leforestier, J. Chem. Phys. **114**, 1685 (2001).
[27] H.-J. Werner and P. J. Knowles, J. Chem. Phys. **89**, 5803 (1988).
[28] P. J. Knowles and H.-J. Werner, Chem. Phys. Lett. **145**, 514 (1988).
[29] T. H. Dunning, Jr., J. Chem. Phys. **90**, 1007 (1989).
[30] S. R. Langhoff and E. R. Davidson, Int. J. Quantum Chem. **8**, 61 (1974).
[31] H.-J. Werner, P. J. Knowles, R. Lindh *et al.*, MOLPRO, version 2002.6, a package of *ab initio* programs (2003). see http://www.molpro.net.
[32] S. Han and D. R. Yarkony, J. Chem. Phys. **119**, 5058 (2003).
[33] M. Baer, Phys. Rep. **358**, 75 (2002).
[34] M. Baer, Adv. Chem. Phys. **124**, 39 (2002).
[35] J. N. Murrell, S. Carter, S. C. Farantos, P. Huxley, and A. J. C. Varandas, *Molecular Potential Energy Functions* (Wiley, Chichester, 1984).
[36] R. Siebert, P. Fleurat-Lessard, R. Schinke, M. Bittererová, and S. C. Farantos, J. Chem. Phys. **116**, 9749 (2002).
[37] S. Yu. Grebenshchikov, R. Schinke, P. Fleurat-Lessard, and M. Joyeux, J. Chem. Phys. **119**, 6512 (2003).
[38] S. F. Deppe, U. Wachsmuth, B. Abel, M. Bittererová, S. Yu. Grebenshchikov, R. Siebert, and R. Schinke, J. Chem. Phys. **121**, 5131 (2004).
[39] J. C. Light and T. Carrington, Adv. Chem. Phys. **114**, 263 (2000).
[40] J. Echave and D. C. Clary, Chem. Phys. Lett. **190**, 225 (1992).
[41] Z. Bačić and J. C. Light, Annu. Rev. Phys. Chem. **40**, 469 (1989).
[42] T. P. Grozdanov, V. A. Mandelshtam, and H. S. Taylor, J. Chem. Phys. **103**, 7990 (1995).
[43] M. R. Wall and D. Neuhauser, J. Chem. Phys. **102**, 8011 (1995).
[44] V. A. Mandelshtam and H. S. Taylor, J. Chem. Phys. **106**, 5085 (1997).
[45] M. Joyeux, S. C. Farantos, and R. Schinke, J. Phys. Chem. A **106**, 5407 (2002).
[46] S. C. Farantos, Zheng-Wang Qu, H. Zhu and R. Schinke (in preparation).
[47] D. H. Katayama, J. Chem. Phys. **71**, 815 (1979).
[48] H. Zhu, Z.-W. Qu, S. Yu. Grebenshchikov, R. Schinke, J. Malicet, J. Brion, and D. Daumont J. Chem. Phys., in press (2004).
[49] J. Malicet, D. Daumont, J. Charbonnier, C. Parisse, A. Chakir, and J. Brion, J. Atmos. Chem. **21**, 263 (1995).
[50] N. Taniguchi, K. Takahashi, Y. Matsumi, S. M. Dylewski, J. D. Geiser, and P. L. Houston, J. Chem. Phys. **111**, 6350 (1999).
[51] S. Yu. Grebenshchikov, R. Schinke, and W. L. Hase, in *Unimolecular Kinetics*, edited by N. Green (Elsevier, Amsterdam, 2003).
[52] J. M. Flaud and R. Bacis, Spectrochim. Acta, Part A **54**, 3 (1998).
[53] K. Takahashi, M. Kishigami, Y. Matsumi, M. Kawasaki, and A. J. Orr-Ewing, J. Chem. Phys. **105**, 5290 (1996).
[54] P. O'Keeffe, T. Ridley, K. P. Lawley, R. R. J. Maier, and R. J. Donovan, J. Chem. Phys. **110**, 10803 (1999).
[55] Rotational broadening is large for absorption in the Huggins band, because the rotational constants in the $X$ and the $B$ state are, as a result of the different geometries, quite different. From calculations for $J=0$ and 1 we derived the following values for the ground vibrational state: $A=2.5085\ \mathrm{cm}^{-1}$, $B=0.3545\ \mathrm{cm}^{-1}$, and $C=0.3145\ \mathrm{cm}^{-1}$.
[56] J. C. D. Brand, K. J. Cross, and A. R. Hoy, Can. J. Phys. **56**, 327 (1978).
[57] J. W. Simons, R. J. Paur, H. A. Webster, III, and E. J. Bair, J. Chem. Phys. **59**, 1203 (1973).
[58] H. Ishikawa, R. W. Field, S. C. Farantos, M. Joyeux, J. Koput, C. Beck, and R. Schinke, Annu. Rev. Phys. Chem. **50**, 443 (1999).
[59] M. Golubistsky and D. G. Schaeffer, *Singularities and Groups in Bifurcation Theory* (Springer, New York, 1981), Vol. I.
[60] E. L. Allgower and K. Georg, *Numerical Continuation Methods, Springer series in Computational Mathematics* (Springer-Verlag, Berlin, 1993), Vol. 13.
[61] S. C. Farantos, Int. Rev. Phys. Chem. **15**, 345 (1996).
[62] S. C. Farantos, Comput. Phys. Commun. **108**, 240 (1998).
[63] M. P. Jacobson and M. S. Child, J. Chem. Phys. **114**, 250 (2001).
[64] M. P. Jacobson and M. S. Child, J. Chem. Phys. **114**, 262 (2001).

**Downloaded 30 Nov 2004 to 139.91.254.18. Redistribution subject to AIP license or copyright, see http://jcp.aip.org/jcp/copyright.jsp**